Development of Magnetically Responsive Multifunctional Nanoparticles for Catalytic Reduction Reactions

A thesis submitted towards the partial fulfillment of BS-MS programme

By Govind S

20131043
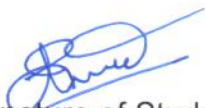
Under the guidance of

Dr. Pramod P. Pillai

Assistant Professor, Department of Chemistry

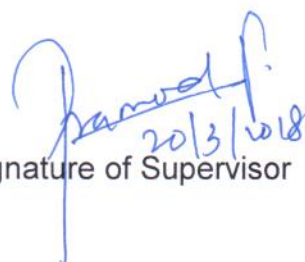*Indian Institute of Science Education and Research*

Pune

Certificate

This is to certify that this dissertation titled 'Development of Magnetically Responsive Multifunctional Nanoparticles for Catalytic Reduction Reactions' towards the partial fulfilment of the BS-MS dual degree programme at the Indian Institute of Science Education and Research, Pune represents study/work carried out by **Govind S** at **IISER, Pune** under the supervision of **Dr. Pramod P. Pillai**, Assistant Professor, Department of Chemistry during the academic year, **2017-2018**.
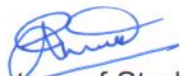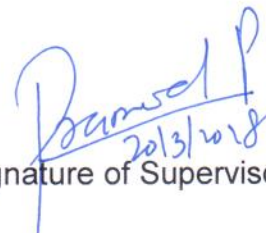
Signature of Student

Signature of Supervisor

20/3/2018

Date: 20|03|2018

Place: Pune

2

Declaration

I hereby declare that the matter embodied in the report titled 'Development of Magnetically Responsive Multifunctional Nanoparticles for Catalytic Reduction Reactions' are the results of the work carried out by me at the Department of Chemistry, IISER, Pune, under the supervision of **Dr. Pramod P. Pillai** and the same has not been submitted elsewhere for any other degree.

Signature of Student

Signature of Supervisor

Date: 20|03|2018

Place: Pune

Acknowledgement

Table of Contents

List of Figures

List of Tables

No	Title	Page No

Abstract

Introduction of multiple functionalities at the nanoscale is a major challenge in the area of nanoscience. Typically, one carries out different kinds of modifications to the nanoparticle systems for the realization of diverse functional traits. One of the most attractive functional trait deals with the emergence of intelligently "*responsive*" behavior from a nanoparticle system. We endeavor into the regime of incorporating advanced functionalities by integrating two attractive nanoscale properties: plasmonics and magnetism. The multifunctional nanohybrid system comprised of Gold (Au) and magnetite (Fe_3O_4) NPs, which imparted the plasmonic and magnetic properties respectively. The work undertaken in this thesis is summarized into three parts. Firstly, we summarize our efforts along with the challenges that we faced in our attempts to synthesize desired Fe_3O_4/Au core/shell NPs. Secondly, we present an alternative synthetic strategy for attaching plasmonic Au NPs on magnetic Fe_3O_4 NPs using an amorphous silica shell as the binder. Thirdly, we explore the multifunctional properties of these $Au@Fe_3O_4/SiO_2$ core/shell NPs in catalysis. The metallic and plasmonic properties of Au NPs in the nanohybrid were used for the catalytic reduction of substrates; whereas the magnetic property of Fe_3O_4 was conveniently used for the separation and recyclability of the catalyst. The $Au@Fe_3O_4/SiO_2$ core/shell NPs exhibited catalytic activity comparable to the commonly used benchmark citrate stabilized Au NP catalyst. At the same time, the multifunctional catalyst developed by us showed superior recyclability and additional advantage of ease of separation.

Chapter 1: Introduction

The major thrust of research being carried out at the nanoscale aims at understanding the behavior that emerges when materials are confined to the nanometer length scale (~1-100nm). As a result of this confinement, known materials starts behaving in unknown and oftentimes, counterintuitive ways. For instance, semiconductors like CdSe, ZnSe, PbSe, InP etc. of suitable sizes starts to glow upon excitation with light. Such materials are called quantum dots (QDs) and are of immense interest for several biomedical applications[1]. Interestingly, one can get all the colors in the visible spectrum from the same material, by an easy and convenient variation in the size of QDs. Contrast this with undertaking the same task at the molecular scale, where one has to synthesize different dyes (chromophores) in order to get different colors. It's not only just semiconductors that behave in curious non-intuitive ways, metal nanoparticles (MNPs) starts to display size and shape dependent absorption properties. Unlike the HOMO-LUMO transitions in molecular systems, the vibrant color in case of MNPs arises from a phenomenon called surface plasmon resonance (SPR). A plasmon is the collective oscillation of the free electrons in the conduction band. So, when electromagnetic radiation (the source of energy) interacts with the free electrons in the metal, the electrons gets polarized and are displaced from their mean position. This leads to the generation of positive charge, which pulls the electrons back, and makes them oscillate on the surface of metals[2]. The plasmons in a nanoparticles are analogous to the mass-spring harmonic oscillator and the only difference is that here the oscillations are driven by resonant energy radiation[3]. The resonance condition is achieved when the incident electromagnetic radiation frequency matches with the natural oscillating frequency of the electrons[2]. For silver (Ag), gold (Au) and copper (Cu), the SPR absorption occurs in visible region, giving rise to their characteristic yellow, wine-red and blue colors respectively. The localized SPR for a metal can be mathematically represented as[4]:-

$$\omega_{sp} = \sqrt{(\omega_p{}^2/1+2\varepsilon_m) - \gamma^2}$$

$$\omega_p = \sqrt{N e^2/\varepsilon_0 m}$$

Where,

ω_{sp} is the surface plasmon frequency

ω_p is the bulk plasma oscillation frequency

ε_m is the dielectric constant of environment

γ is the line width of surface Plasmon band

N is the density of free carriers

m is the mass of the charge carrier

SPR heavily depends on the size, shape, environment, etc. of the host NP[3]. For instance, AuNPs display a vibrant wine-red color, while gold nanorods (AuNRs) display a blue color: two different colors from the same material (Au) differing in shape (**Figure 1.2**). The color in the case of AuNRs can be tuned easily by a convenient variation in the lengths of the nanorod. Here, the effect of modifications in size of NPs on SPR is analogous to the change in elastic constant of the harmonic spring[3], which affects the oscillation frequency, resonance condition and ultimately, the color of NPs. Moreover, the sensitivity of SPR to the environment serves as a great non-destructive identification tool for different analytical and biochemical reactions. This has led to

Figure 1.1|Optical photograph showing the variation in the color of gold nanorods (AuNRs) with a change in their sizes.(Adapted from reference 5)

the development of a new spectroscopic technique, called SPR spectroscopy. Curiously, the extinction coefficient of MNPs is 10^4– 10^5 times higher than the best-known organic dyes[6], which makes them an attractive material for light absorption,

sensing and imaging applications. For instance, colorimetric sensing with AuNPs is quite popular since the binding of various analytes on nanoparticle leads to the aggregation of NPs, leading to color change because of interparticle SPR coupling[3]. Also, the confinement of electric field (because of SPR) within a small metallic sphere is also responsible for the host of properties that have made AuNPs famous and attractive for research purposes. For instance, MNPs upon excitation by an optical wave, lead to a prominent enhancement of electric field in its vicinity (MNPs act as nano-lenses for the electromagnetic radiation[3]). This enhanced electric field makes MNPs attractive for applications like Surface Enhanced Raman Spectroscopy (SERS). Generally, the efficiency of Raman scattering is very low in molecules and this efficiency can be drastically improved if the molecules are in proximity to plasmonic nanoparticles[3]. The reason for the enhancement in intensity is due to electromagnetic enhancement, which occurs when the electric field of surface plasmons interacts with the transition dipole moment of the adsorbed molecule. The other major factor for the enhancement is chemical enhancement occurs due to the mixing of metal and molecular orbitals[2]. Another well-known and yet counterintuitive application of AuNPs relies on catalysis. Although bulk Au is viewed as an inert metal, AuNPs are known to act as a catalyst for several known reactions like oxidation of CO[6], reduction of aromatic amines, photocatalytic reduction of potassium ferricyanide, etc.

It is worthwhile to point out that most of the properties displayed by AuNPs (mentioned above) are not based on individual NPs, but rather on purposeful assemblies of the NPs. This leads to the fascinating challenge of being able to assemble/manipulate them in useful ways. For instance, the otherwise arduous task of separating MNPs after catalysis can be easily overcome if we could *switch-on* the interactions between NPs leading to their precipitation, and hence, separation from the reaction system. In this direction, researchers have started to control the interactions between NPs by controlling functionalities that are displayed at their surfaces. Among different forces, the use of magnetic forces is interesting in particular. The central idea of the present thesis therefore is to investigate the effects of magnetic forces on the catalytic efficiency of AuNPs. In doing so, we are entering into the domain of a multifunctional plasmonic-magnetic hybrid NP system.

Our attempts to use magnetic forces for the manipulation of plasmonic NPs led us to the domain of magnetic NPs. These magnetic NPs are attractive for their useful applications in high density storage of data, for magnetic separations, drug delivery, hyperthermia treatments and so on[7]. Significant progress has been made in the chemical wet synthesis of highly monodisperse magnetic particles (metals, alloys etc.) in the past few years[8]. Among different magnetic NPs available, iron oxide nanoparticles (Fe_3O_4 NPs) have been a hot topic because of its biocompatibility and non-toxicity. Moreover, having a Au shell over Fe_3O_4 NPs gives us a great handle to tune the non-trivial surface chemistry of Fe_3O_4 NPs.We therefore thought of integrating magnetism and plasmonics into a single system.

Our initial efforts on the synthesis of Fe_3O_4/Au core/shell NP system failed to yield the desired integration of plasmonic and magnetic properties. We then modified our synthetic strategy and took the aid amorphous silica as a binder to connect Fe_3O_4 and Au NPs. Here, we coated Fe_3O_4 NPs with a mesoporous SiO_2 shell, which was functionalized with appropriate surface ligands for feasible chemisorption of AuNPs.The multifunctional properties of these Au@Fe_3O_4/SiO_2 core/shell NPs were employed in catalysis studies. The metallic and plasmonic properties of Au NPs are used for the catalytic reduction of substrates; whereas the magnetic property of Fe_3O_4 was conveniently used for the separation and recyclability of the catalyst. The Au@Fe_3O_4/SiO_2 core/shell NPs exhibited catalytic activity comparable to the commonly used benchmark citrate Au NP catalyst. At the same time, the multifunctional catalyst developed by us showed superior recyclability and additional advantage of ease of separation.The prepared multifunctional materials displaying both magnetic and plasmonic properties will have long lasting impacts in the field of material science.

Chapter 2: Materials and Methods

2.1. Experimental Section

2.1.1. Materials and Reagents: $FeCl_3.6H_2O$, Octadecene (99%), Dodecylamine (DDA), Sodium citrate tribasic dihydrate, $FeCl_2.4H_2O$, 4-Nitrophenol, NH_4OH (28% in H_2O), Tetraethylorthosilicate (TEOS), 3-(aminopropyl)triethoxysilane (APTES), Oleic acid, NaOH pellets were purchased from Sigma Aldrich and used as received. All the chemicals were used without any further purification.

2.1.2. Synthesis of Fe_3O_4 nanoparticles: Synthesis of Fe_3O_4 nanoparticles were carried out by the thermal decomposition of Fe(III)-oleate and oleic acid. Fe(III)-oleate was prepared according to the reported procedure[9]. In a typical experiment, 3.2 g of $FeCl_3.6H_2O$ (12 mmol.) was dissolved in 12 mL distilled water and filtered. The solution was then mixed with 10.95 g (36.0mmol.) of sodium oleate, 24mL of ethanol, 6mL of distilled water and 42 mL of hexane and heated up to $70°C$ under vigorous stirring for 4 hours. After the completion of reaction, the upper reddish brown layer containing Fe(III)-oleate was separated and washed with distilled water 3 times. Hexane was evaporated using rotary evaporator and the product was placed under vacuum for drying. The as synthesized Fe(III)-oleate solution was used for the synthesis of Fe_3O_4 nanoparticles according to a reported protocol[9]. Briefly, 1.92 g (3.0mmol.)of Fe(III)-oleate, 1.54 mL of oleic acid (4 mmol.) and 6.62 mL of octadecene were added to a RB containing a magnetic stir bar. The solution was then heated to $320°C$ under stirring. The color of solution changed from reddish brown to blackish red while heating. Upon reaching $320°C$, the solution was then air refluxed for 20 min and cooled down to room temperature. Once the reaction was completed, it was allowed to cool down to room temperature and precipitatation of NPs were done with 1:4 mixture of hexane and acetone, and separated by centrifugation. The nanoparticles were then redispersed in toluene.

2.1.3. Synthesis of Fe_3O_4/Au core/ shell NPs in toluene: Core/shell nanoparticles were synthesized by modifying the reported procedure[11].Synthesis began with the phase transfer of Au salt ($HAuCl_4.3H_2O$ in our case) to toluene using DDA (**Figure 2.1**).

In a typical experiment, 10 mL of 1 mM Au (III) was mixed with 10 mL of ethanol containing 0.2mL of DDA (0.87 mmol, 161 mg). The solution was then stirred for 5 minutes and 5 mL toluene was added. The mixture was then stirred for overnight to ensure the complete phase transfer of gold from water to toluene. Once the reaction was completed, Au (III) in toluene was separated from the aqueous layer and used for the over coating reaction.
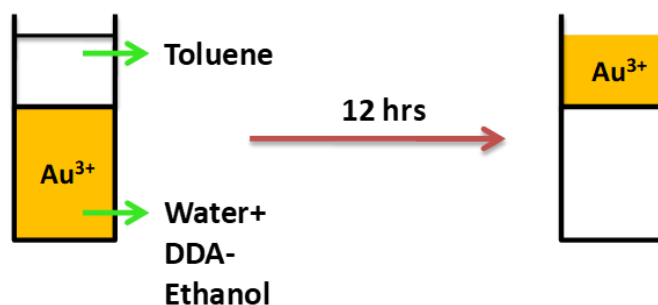
Figure 2.1| Schematic illustration of the phase transfer protocol of Au(III) from aqueous phase to toluene phase. We used an ethanolic solution of dodecylamine (DDA) to coordinate with Au(III) and phase transfer it to toluene phase.

Au coating was carried out using a seed mediated reduction method, where Fe_3O_4 NP in toluene were used as seeds for the growth of Au shell[11]. Briefly, 5mL of 1mM Fe_3O_4 NPs (seed solution) was heated to $80°C$ under stirring for 5 minutes, and Au(III)-DDA (5mL) in toluene was then added to the seed solution and stirred at $80°C$ for 6 hours. The solution color was changed from golden yellow to dark red over the course of reaction.
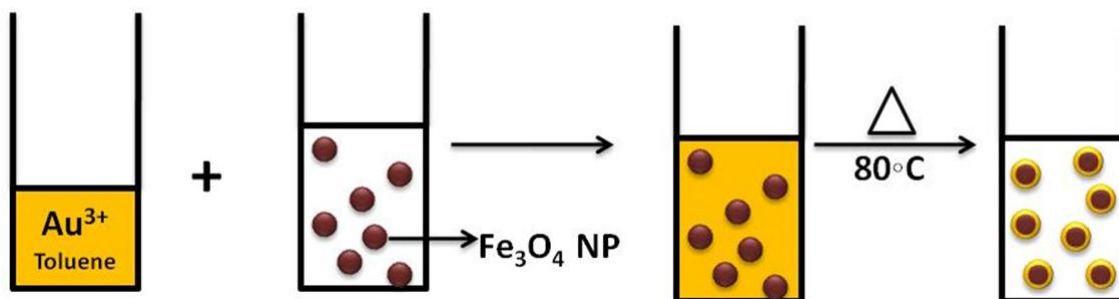
Figure 2.2| Schematic illustration of growth of Au shell onto Fe_3O_4 NPs in toluene.

2.1.4. Synthesis of water soluble Fe_3O_4 nanoparticles: Water soluble Fe_3O_4 nanoparticles were synthesized by co-precipitation method according to the existing

literature[10]. 4 g of $FeCl_2.4H_2O$ (20 mmol) and 10.12 g of $FeCl_3.6H_2O$ (40 mmol) were dissolved in 360 mL of deionized water and 56 mL of NH_4OH (30%) was added rapidly to it. After 2 minutes, 12.6 g of citric acid monohydrate (60 mmol) was added to it and the solution was then transferred to a glass beaker. It was then sonicated for one hour. After the completion of reaction, the Fe_3O_4 nanoparticles were sedimented using a magnet and the brown color supernatant was discarded. Acetone was added and again kept for sonication. This process was repeated four times.The nanoparticles after purification were redispersed in water and kept it $60°C$ for evaporating the traces of acetone present.

2.1.5. Synthesis of Fe_3O_4/Au core/shell NPs in water: The synthesis of Fe_3O_4/Au core/shell NPs were carried out according to the reported protocol[12]. 0.35mL of as synthesized water soluble Fe_3O_4 nanoparticles (0.1M) was added to boiling water under vigorous stirring. ~ 0.7 mL of 10 mM Au (III) was added, followed by the addition of 0.3mL sodium citrate (0.1 M). The solution was heated and stirred for 20 minutes and was then cooled down to room temperature on its own. The color of the solution changed from black to wine red during the reaction. The solution was then used for further studies.

2.1.6. Synthesis of Fe_3O_4/SiO$_2$ core/shell nanoparticles: Fe_3O_4/SiO$_2$ core shell particles were synthesized by a modified procedure[13,14]. In a typical experiment, 47.25 mg of Fe_3O_4 synthesized via high temperature thermal decomposition method was redispersed in 3.15 mL toluene and was mixed with 50 mL of ethanol, 12 mL of distilled water and 1.6 mL of NH_4OH. The solution was stirred at room temperature for 20 minutes. Subsequently, 0.63 mL of TEOS was added dropwise to the solution under stirring. The mixture was then heated to $75°C$ and stirred for 4 hours. The Fe_3O4/SiO_2 NPs oxide core shell nanoparticles were collected via magnetic separation and re-dispersed in ethanol.

2.1.7. Surface functionalization of Fe_3O_4/SiO$_2$ core shell NP: The silica shells were functionalized with 3-(aminopropyl)triethoxysilane (APTES) according to the reported literature[15]. 38.5 mg of Fe_3O_4/SiO$_2$ NPs were dissolved in 67.3 mL ethanol and sonicated for 20 minutes. 0.38 mL of APTES was added to the solution and was stirred

at 80°C for 5 hours. The resultant particles were collected via magnetic separation, washed three times with ethanol and redispersed in water.

2.1.8. Synthesis of citrate stabilized Au nanoparticles: Citrate stabilized AuNPs were prepared according to the well-known protocol[16]. Briefly, 10 mL of 1mM $HAuCl_4.3H_2O$ was prepared and heated it to boil. 1 mL of 1% sodium citrate tri basic solution is then added to the boiling gold solution under stirring. Heating was continued until the color change to wine red was evident.

2.1.9. Synthesis of Au@Fe_3O_4/SiO_2 NPs: Au coating over Fe_3O_4/SiO_2 core/ shell NPs were carried out according to the reported literature[17]. In a typical experiment, 1 mL of citrate stabilized AuNP (~60nM in terms of AuNPs) was added to 0.5 mL aqueous solution of Fe_3O_4/SiO_2 core/ shell NPs (1mg/mL) under sonication and the mixture was sonicated for five minutes. The resultant particles were separated via magnetic separation, washed with water several times and re-dispersed in water.

2.1.10. Catalytic reduction of 4-Nitrophenol (PNP): The catalytic reduction was carried out by adding 4 µL of PNP (5mM), 200 µL of $NaBH_4$ (0.1M), 0.5 mL of Au@ Fe_3O_4/SiO_2 NP solution and 1.5 mL of milliQ water in a 3 mL Quartz cuvette[18]. Time dependent absorption measurements were done using a UV-Vis.-NIR spectrophotometer. Control experiments were done using citrate stabilized AuNPs as well as Fe_3O_4/SiO_2 NPs.

2.1.11. Photo catalytic reduction of [Fe(CN)$_6$]$^{3-}$: The catalytic reductions were monitored under UV-VIS spectroscopy. In a typical experiment, Au@Fe_3O_4/SiO_2 NPs (absorbance was set to ~1), 0.88 mL EtOH (5M), 50 µL of K_3[FeCN$_6$](30 µM) were added and mixed in a 3 mL Quartz cuvette and kept it under Ar flow for 15 minutes[19]. The cuvette was sealed with Teflon and kept it under room temperature. Photocatalytic reduction was carried out by irradiating the sample with blue LED (1 W). Reduction was measured by monitoring the absorbance of ferricyanide ion at 15 min interval for around 1.5 hours at fast scan mode. Gradual decrease in the peak around 420 nm showed the reduction of [Fe(CN)$_6$]$^{3-}$.

2.2 Characterization Techniques

2.2.1 Dynamic Light Scattering (DLS) studies: Hydrodynamic radius of the nanoparticle systems were estimated using dynamic light scattering studies. The measurements were taken in ZetasizerZS90 Malvern instrument. For DLS measurements, samples were diluted in proper solvents and measurements were done. Data from three measurements were averaged and size v/s intensity distributions were recorded.

2.2.2 UV-Vis absorption studies: Absorption studies were carried out in SHIMADZU UV-3600 plus UV-VIS NIR spectrophotometer. Samples were diluted and absorption was monitored over the entire visible range of 400-800 nm. The concentration of nanoparticles was calculated from Beer-Lambert law.

$$A = \varepsilon.c.L$$

where, A: optical density at the absorption maxima

ε: Molar extinction coefficient at a particular wavelength (For Au NP, ε = 5.14 x 10^7)[18]

c: Concentration of solution

L: optical path length

For catalysis experiment, reductions were carried out in a 3 mL Quartz cell of path length 1 cm. Nanoparticle solutions, $NaBH_4$ & PNP were mixed and absorption was monitored from 250-800 nm. For checking the kinetics, time scan measurements were taken at every minute. Time dependent kinetics was also investigated by monitoring the absorbance. Catalysis experiments were carried out at ambient conditions.

2.2.3 Microscopy Studies:

2.2.3.1 Transmission Electron Microscopy: Samples were diluted and then drop casted on a 400 mesh carbon coated Cu grid (Tadpellalnc) and kept it under vacuum for proper drying. The High Resolution Transmission Electron Microscopic (HRTEM) imaging was performed on TECNAI G2 20 TWIN at 200 kV

2.2.3.2 Scanning Electron Microscopy: Samples were diluted and then drop casted on a Si wafer and kept it under vacuum for proper drying. The FESEM imaging was performed on ZEISS GEMINI FESEM.

2.2.4. Product Characterization: The products formed after reduction was characterized by ^{1}H NMR and HRMS techniques. After the reduction, the product was then passed through a celite column for separating the product from nanoparticles and excess sodium borohydride. The product was then extracted using ethyl acetate and was dried using sodium sulfate. Solvent was evaporated using rotary evaporator to yield solid product. The NMR spectrum was collected in deuterated DMSO (JEOL 400MHz). The HRMS spectrum was obtained using Water's SYNAPP-G2 instrument.
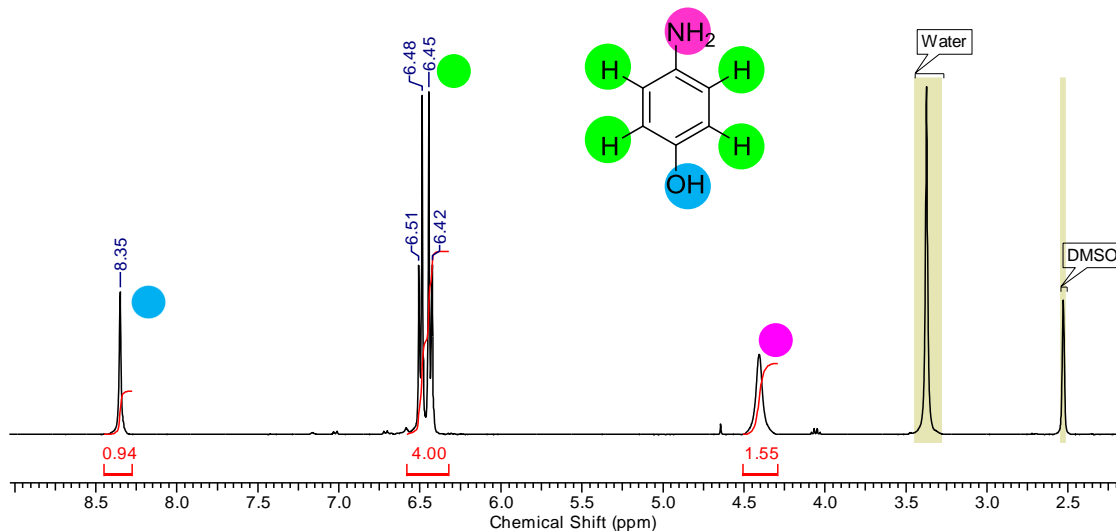
Figure 2.3l[1]H-NMR spectrum of 4-aminophenol (the product, PNA) that was produced by the catalytic reduction of 4-nitrophenol (the reactant, PNP) by Au@ Fe_3O_4/ SiO_2 NPs.
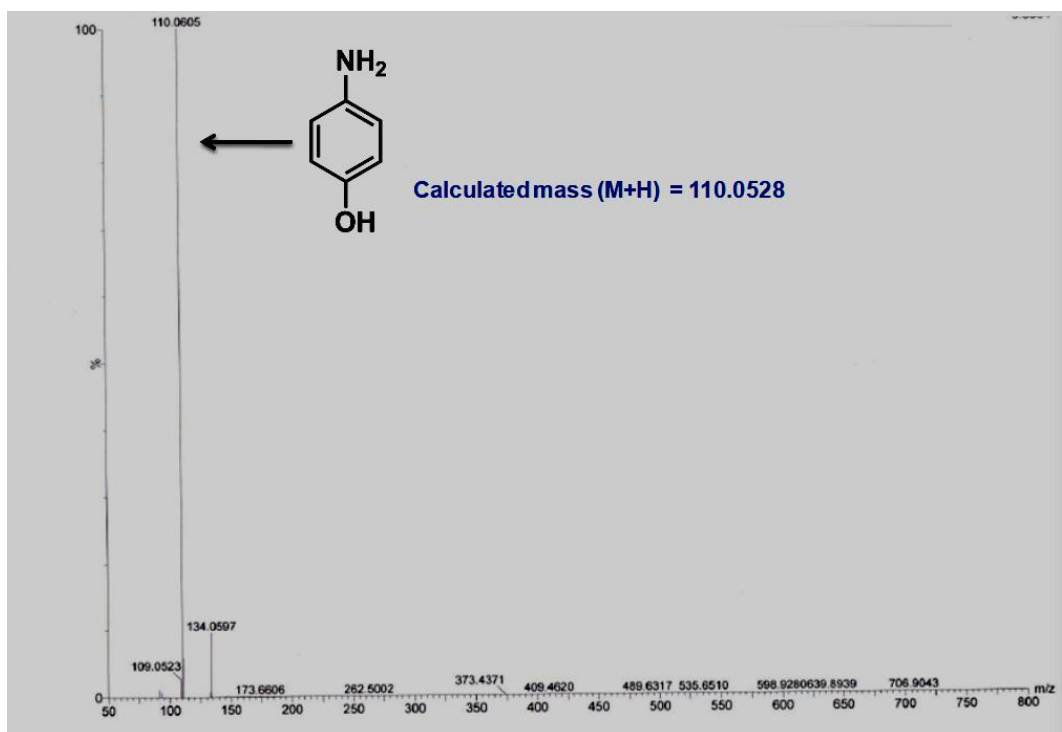
Figure 2.4I HRMS spectrum of 4-aminophenol (the product, PNA) that was produced by the catalytic reduction of 4-nitrophenol (the reactant, PNP) by Au@ Fe_3O_4/ SiO_2 NPs.

2.3. Calculations

2.3.1. Calculation of kinetic rate constants:

PNP Reduction: Analysis was done according to the pseudo-first order rate equation. Concentration of PNP at each time was calculated by analyzing the absorbance of PNP at ~400 nm using the Beer-Lambert's law. The linear correlation between $-\ln(c_t/c_0)$ and reaction time was investigated for determining the rate constants, where c_0 is the initial concentration of PNP and c_t is the concentration of PNP at time t. Rate constant was determined from the slope of plot.

Photocatalytic Reduction of $[Fe(CN)_6]^{3-}$: In order to calculate the rate constant we used first order rate equation ($-\ln(c_t/c_0)$ v/s time) as in the previous case. The decrease in $[Fe(CN)_6]^{3-}$ absorbance at ~420 nm was plotted against time to calculate the rate constant.

Chapter 3: Results and Discussion

3.1 Preparation of Fe$_3$O$_4$/Au Core/Shell Nanoparticles

In order to meet our overarching aim of integrating plasmonic as well as magnetic properties into a single structure, we employed two different synthetic strategies. According to our first strategy, we aimed to grow a shell of Au over Fe$_3$O$_4$ NPs resulting in a core/shell NP geometry.Secondly, we thought of introducing an amorphous SiO$_2$ layer between Fe$_3$O$_4$ and Au for favorable conjugation of the two materials. The resulting structures from both the strategies will demonstrate the presence of plasmonic as well as magnetic properties.

Fe$_3$O$_4$ NP
Easy Separation
Non toxic
Biomedical applications

Au NP
Well defined Surface chemistry
Plasmonic features
Biocompatibility
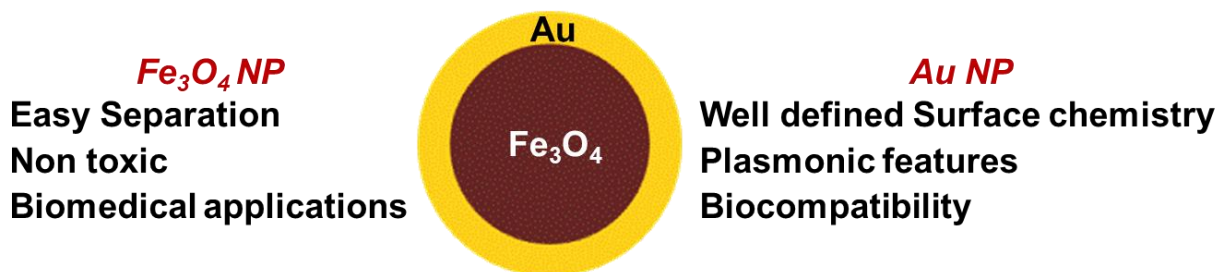
Figure 3.1| Scheme showing the multifunctional magnetic/plasmonic core/shell NP system. This proposed system, neatly integrates the advantages of both plasmonic as well a magnetic NPs.

Strategy I: We envisaged the use of Fe$_3$O$_4$ nanoparticles to act as nucleation centers for the growth of Au shell.

3.1.1. Fe$_3$O$_4$/Au core shell nanoparticles in toluene: We synthesized Fe$_3$O$_4$ NPs having a core diameter of 11.5 $\pm$ 1.2nm (**Figure 3.2(a), (b) and (c)**) using high temperature thermal decomposition of Fe (III)-oleate in the presence of oleic acid. This strategy of thermal decomposition of Fe compounds containing oxygen yields nanoparticles with a narrow size distribution. This is due to the fact that both nucleation and growth processes occur at two different temperatures. Furthermore, by changing the reaction conditions (like temperature, Fe(III): oleic acid ratio, etc.), one can tune the size of the nanoparticles formed. For more details on the synthesis of Fe$_3$O$_4$ NPs, see Experimental Section. The synthesized nanoparticles showed a good response to magnet as shown in **(Figure 3.2(d))**.
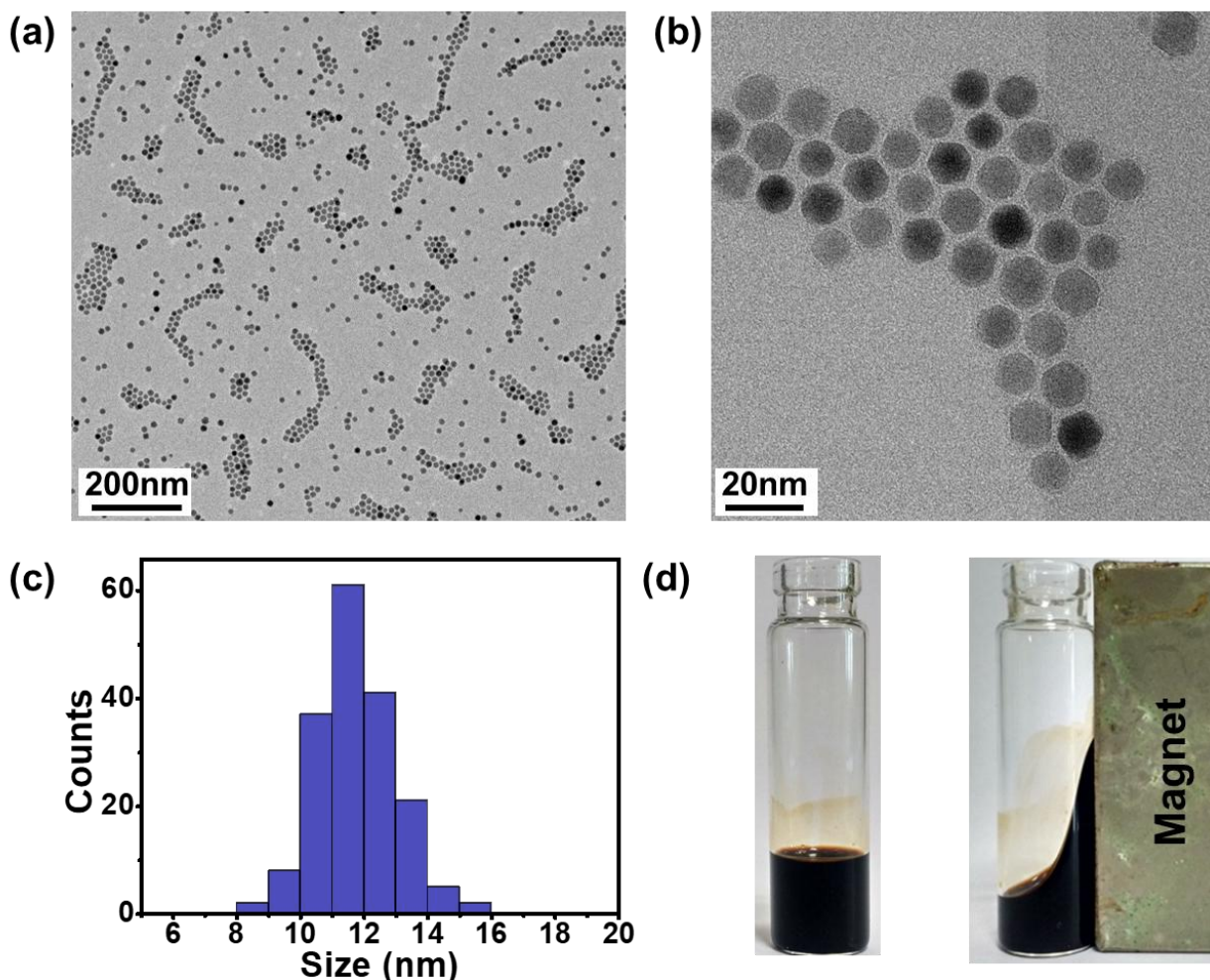
Figure 3.2| Representative TEM images of Fe_3O_4 NPs under **(a)** low magnification, and **(b)** under high magnification.**(c)** Histogram showing the size distribution of synthesized Fe_3O_4 NPs. TEM image analysis was performed on ~150 NPs gave the size to be 11.5 $\pm$ 1.2nm.**(d)** Optical photographs showing the response of Fe_3O_4NPs dispersed in toluene in the absence as well as presence of a magnet.

In order to perform Au over-coating in the organic phase (toluene), we had to employ a phase transfer protocolso as to transfer the Au salt ($HAuCl_4.3H_2O$ in our case) to the organic phase. We used an ethanolic solution of dodecylamine (DDA) to transfer the Au(III)-DDA coordinated species from aqueous to the toluene phase (For details, see Experimental Section). Au solution, thus formed was then employed to synthesize Fe_3O_4/Au core/shell NPs by seed mediated growth[11]. We used Fe_3O_4 NPs to act as the nucleation centers for the growth of Au shell by heating the toluene solution of Au(III)-DDA species in the presence of Fe_3O_4 nanoparticles (For details, see Experimental Section). The solution color was changed from black to wine red during the reaction

suggesting the formation of AuNPs. We precipitated the structure thus formed under the influence of magnetic field. The Fe_3O_4 NPs got precipitated and moved towards the magnet leaving a wine red solution. This observation suggested that the system contained individual Au and Fe_3O_4 NPs, and not Fe_3O_4/Au core/shell geometry.**Figure 3.3**is the UV-Vis absorption spectrum of magnetically isolated NPs which showed the absence of any surface plasmon resonance peak. The finding was further confirmed by inability to phase transfer the synthesized NPs to the aqueous phase with thiols,which are known to have a high binding affinity towards Au.
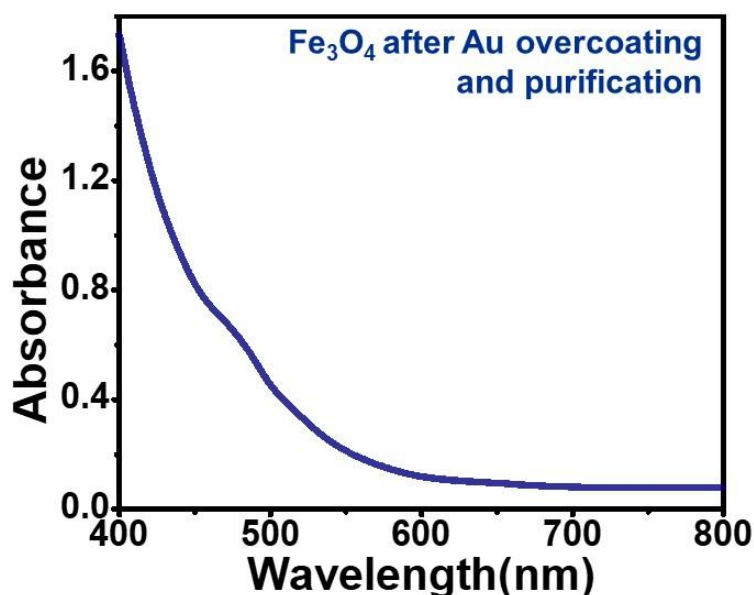
Figure 3.3| Absorption spectra of oleic acid capped Fe_3O_4 nanoparticles after the gold coating attempt.

Alternatively, we hypothesized to form Au shell on Fe_3O_4 NPs (dispersed in water) in the presence of a weak reducing agent (citrate in our case).

3.1.2. Fe_3O_4/Au core/shell nanoparticles in water: We synthesized Fe_3O_4 NPs by utilizing the co-precipitation method[10]. The representative TEM image of the formed Fe_3O_4 nanoparticles along with their response to the magnet is shown in (**Figure 3.4(a), and (b)** respectively).
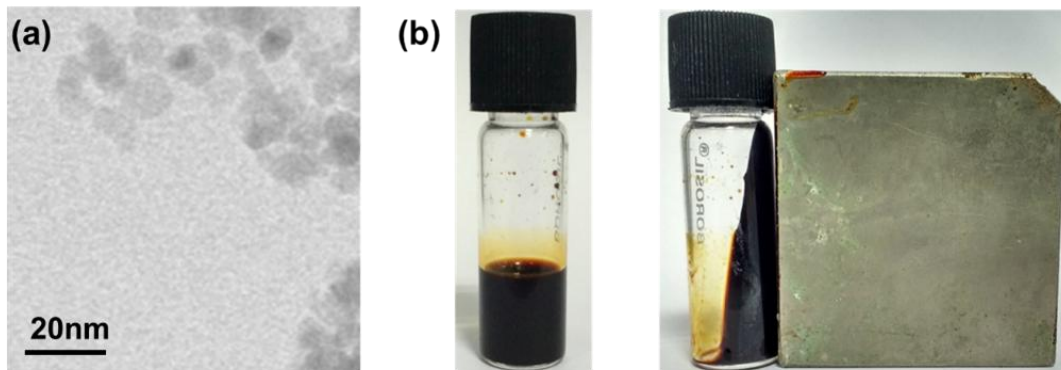
Figure 3.4| (a) Representative TEM image of citrate capped Fe_3O_4 nanoparticles dispersed in water. **(b)**Optical photographs showing the response of Fe_3O_4NPs dispersed in water in the absence as well as presence of a magnet.

We envisaged to have a direct Au coating over citrate capped Fe_3O_4 NPs by using citrate as the reducing agent. According to this procedure, the Au layer synthesis is carried out by mixing Fe_3O_4 NPs with boiling $HAuCl_4$ solution, and under vigorous stirring conditions. The sodium citrate solution is then introduced to the boiling mixture. Sodium citrate acts as both reducing agent as well as providing a citrate surface capping to Fe_3O_4/Au core/shell NPs, thereby rendering the NPs stable. During the reduction of Au(III), the color of the solution was transformed from black to wine red, which indicated the formation of gold nanoparticles. **Figure 3.5(a)** shows the UV-Visible absorption data of both Fe_3O_4 and Fe_3O_4/Au core/ shell NPs. The as synthesized Fe_3O_4/Au core/shell NPs clearly show absorption maxima ~520 nm **Figure 3.5 (a)**. TEM investigations carried out on the prepared sample showed phase separated Au as well as Fe_3O_4NPs as shown in (**Figure 3.5 (b), (c)**).
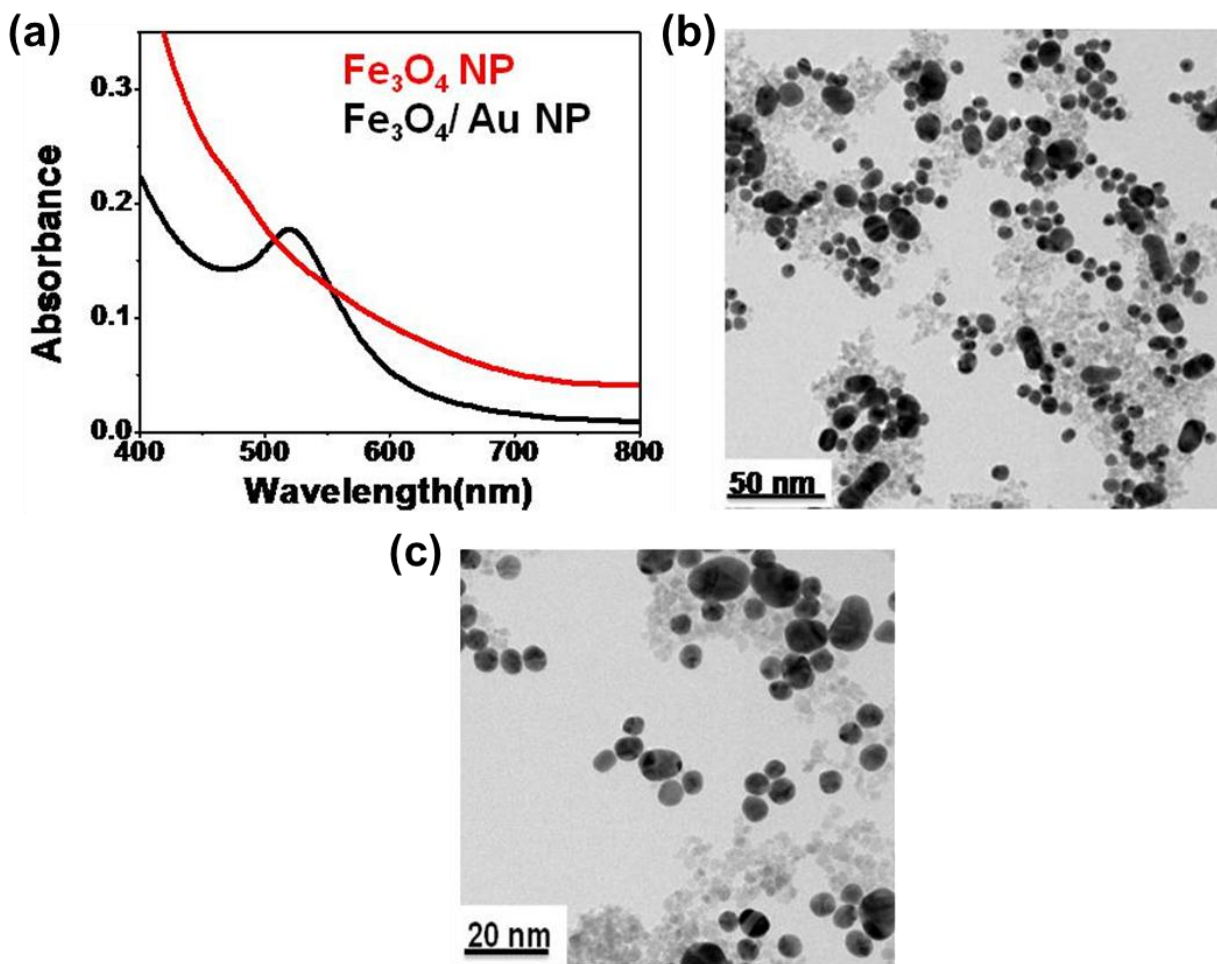
Figure 3.5| (a) Absorption spectra of citrate capped Fe_3O_4 nanoparticles before (shown in red) and after gold coating attempt (shown in black). **(b), (c)** TEM images of the prepared sample showing phase separated Au (dark contrast nanoparticles) and Fe_3O_4 nanoparticles (light contrast nanoparticles).

The inability to form Fe_3O_4/Au core/shell NPs is possibly due to the high lattice mismatch between Au and Fe_3O_4 NPs, and is in accordance with the values reported in literature[20]. Lattice mismatching happens when two different materials having dissimilar lattice constants are brought together by depositing one over the other. Although there have been a few reports on the synthesis of Fe_3O_4/Au NP core/shell structure,the strategies typically require copious amounts of Au salt, ultimately rendering the process uneconomical.

Strategy 2: Using an amorphous layer of SiO₂ on Fe₃O₄ NPs so as to relax the lattice mismatch condition.

Overview: As the presence of high lattice mismatch between Fe_3O_4 and Au prevented them to sit on top of each other into a core/shell geometry, we thought of using an amorphous layer of silica (SiO_2) to conjugate the two materials together. The amorphous layer of SiO_2 can be grown on Fe_3O_4 NPs, and chemically modified so as to stick AuNPs onto it. This will lead to the formation of a hierarchical structure containing both magnetic as well as plasmonic properties. The schematic illustration of our synthesis methodology is given in **Figure 3.6.**The as synthesized material was used as a heterogeneous catalyst for metal NP catalyzed reductions.
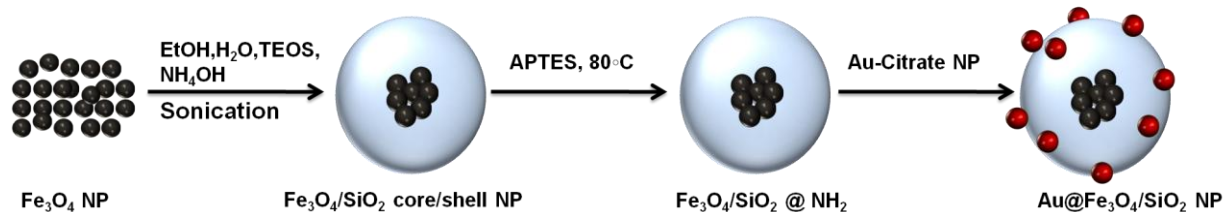
Figure 3.6|Schematic illustration of the synthesis of Au@ Fe_3O_4/SiO_2 NPs.

3.2.1. Synthesis of Fe₃O₄ / SiO₂ core/ shell NPs: Fe_3O_4 NPs were synthesized by high temperature thermal decomposition of Fe(III)-oleate(as discussed before, See Experimental details). We then covered the Fe_3O_4 NPs with a uniform layer of SiO_2 shell using a modified Stöber process. Briefly, oleic acid capped Fe_3O_4 NPs were added to ethanol-water mixture resulting in the formation of an emulsion. In ethanol-water mixture, Fe_3O_4 NPs self-assembled of into clusters due to hydrophobic interactions. Fe_3O_4 clusters acted as nucleation centers and were then covered with a uniform shell of SiO_2 by the base catalyzed hydrolysis, and condensation of tetraethylorthosilicate (TEOS, a silica precursor). The prepared core/shell structure was then visualized with the help of SEM **Figure 3.7 (a), (b)**.Note the contrast in **Figure 3.7 (b)**indicates the compositional differences present in the core as well as shell material of an individual Fe_3O_4/SiO_2 NP. We can see this contrast by looking at the backscattered electrons, which carry information regarding the compositional identity of the material. **Figure 3.7 (c)** shows the Energy Dispersive X-Ray Spectroscopy (EDS)spectrum showing the

presence of both Si as well as Fe in our geometry, further confirming the incorporation of Fe_3O_4 inside the SiO_2 shell.
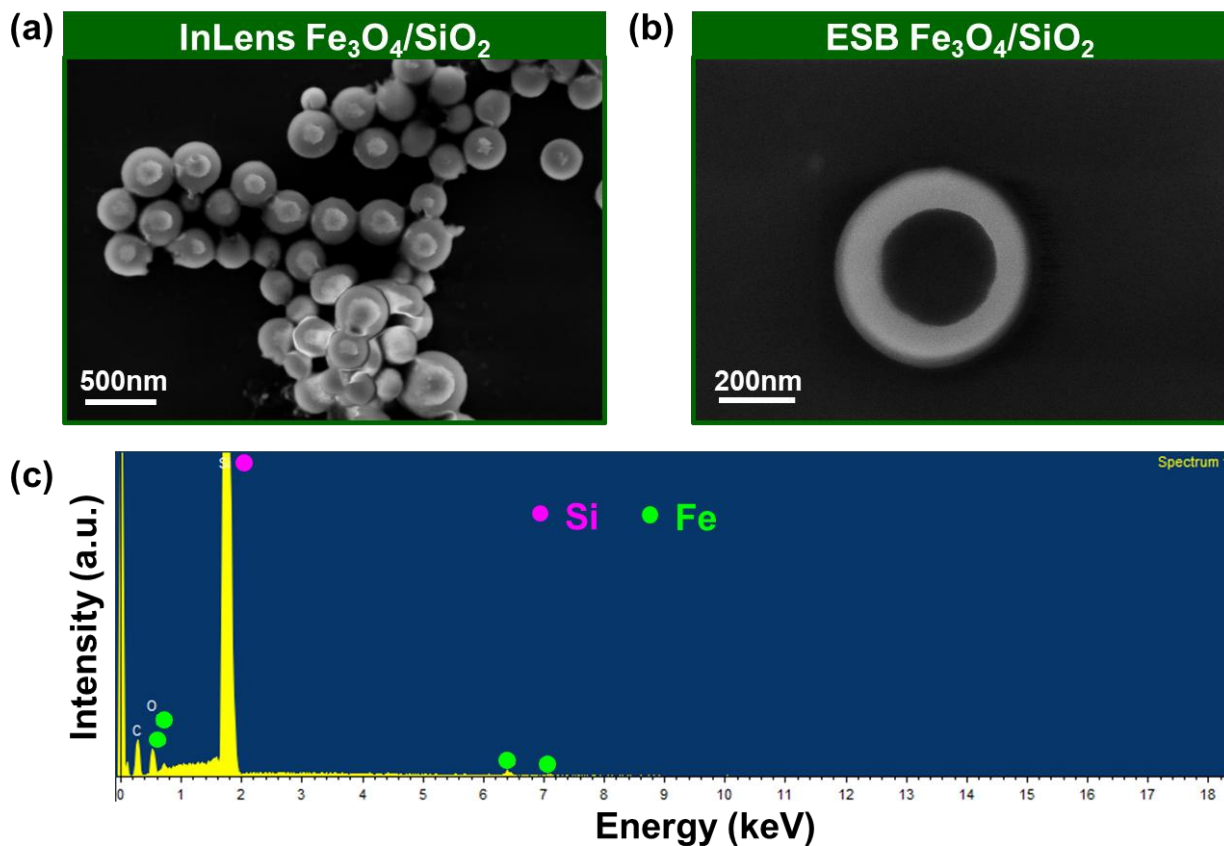
Figure 3.7| (a) Representative SEM images of the Fe_3O_4/SiO_2 core shell nanoparticles. Fe_3O_4 nanoparticles were aggregated during core shell synthesis.The silica shell was synthesized over the aggregated magnetic nanoparticles.**(b)** SEM image of Fe_3O_4/SiO_2 NPs taken using the backscattered electron detector, thereby giving compositional information of the core/shell geometry. Here, the darker areas are Fe_3O_4 NPs, while the lighter outer shell is SiO_2. **(c)**EDS spectrum of Fe_3O_4/SiO_2 core/shell NPs confirming the presence of both Si and Fe.

3.2.2. Au coating over Fe_3O_4/SiO_2 core shell NPs: In order to attach AuNPs to the prepared core-shell geometry, we had to chemically modify the surface of the SiO_2 shell[15]. Accordingly, we functionalized the SiO_2 shell with 3-(aminopropyl)triethoxysilane (APTES), and citrate capped AuNPs were allowed to chemisorb onto it. The synthesis of the hierarchical structure containing AuNPs, SiO_2, and Fe_3O_4 NPs (hereby called, Au@Fe_3O_4/SiO_2 NPs) was driven by the strong affinity of Au with amine. The prepared structure showed the presence of plasmonic band as can be seen from the wine red

color of the solution (**Figure 3.8 (a)**), and the characteristic plasmonic peak at ~ 535nm in the UV-Vis. spectrum (**Figure 3.8 (b)**).**Figure 3.8 (b)** shows the comparison of absorption spectra of bare Fe_3O_4 NP, Fe_3O_4/ SiO_2 core/shell NPs and Au@Fe_3O_4/SiO_2 core/ shell NPs. It should be noted that the AuNPs on the surface of Fe_3O_4/SiO_2 NPs, showed a bathochromic shift of ~15nm, indicating aggregation of NPs on the surface of SiO_2 (**Figure 3.8 (c)**). Along with the presence of plasmons, the prepared structure, due to the presence of magnetic core, showed attractive response in the presence of magnet (**Figure 3.8 (a)**).**Figure 3.8 (a)** clearly shows the plasmonic solution responding to the presence of a magnet, indicating the formation of desired structure. Further confirmation was gained by visualizing Au@Fe_3O_4/SiO_2 NPs using Scanning Electron Microscopy (SEM) (**Figure3.8(d)**). Here, we can clearly see the presence of small AuNPs over Fe_3O_4/ SiO_2 NPs. Presence of AuNPs in our hierarchical structure is further confirmed by the presence of Au peaks in the EDS spectrum (**Figure 3.8 (e)**).
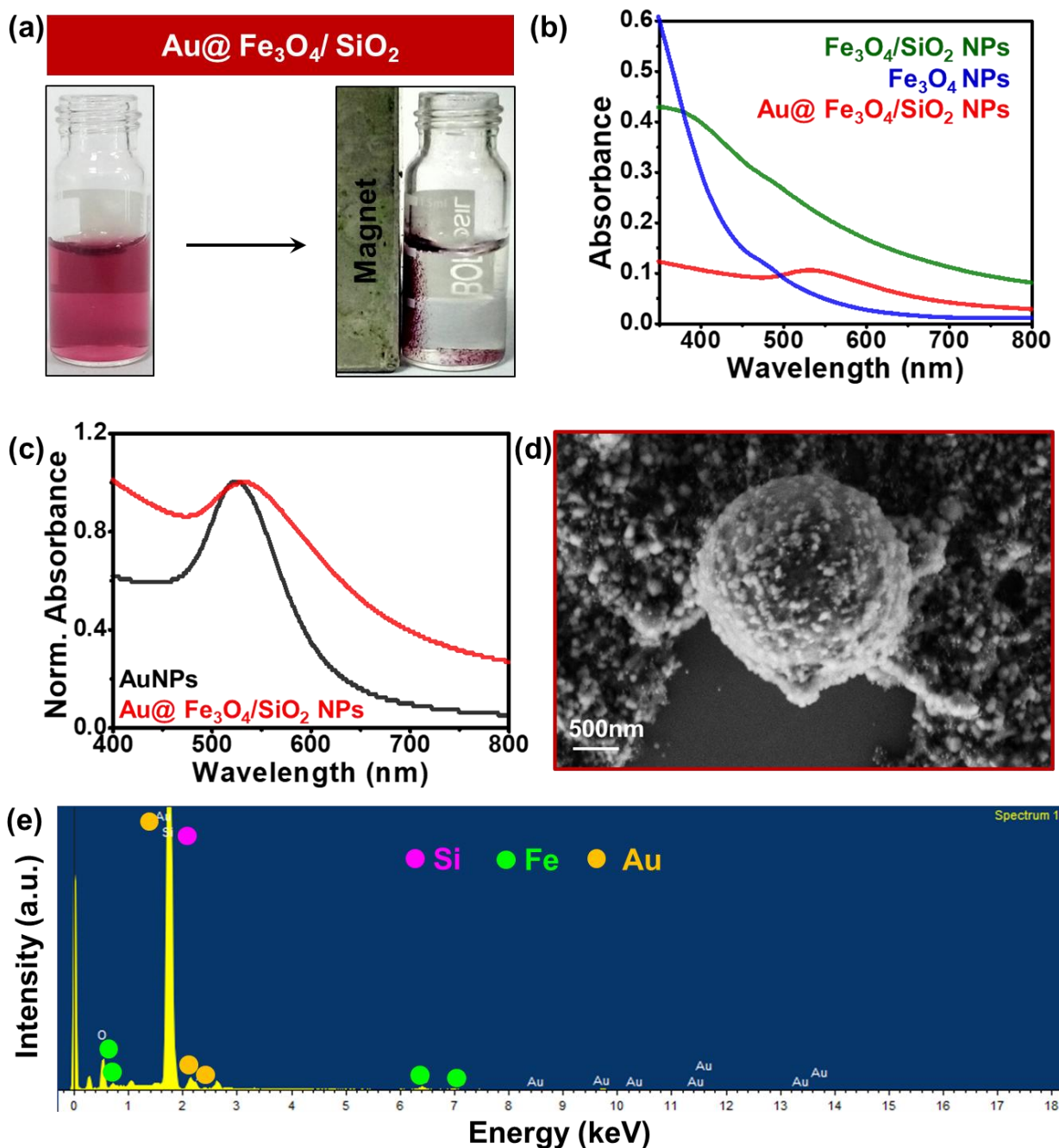
Figure 3.8| (a) Response of Au@Fe_3O_4/SiO_2 core shell nanoparticles under the influence of a magnet. Displacement of the plasmonic solution towards the magnet clearly shows that the as synthesized structure displays both magnetic as well as plasmonics properties. **(b)** UV-Vis spectrum showing the absorbance of Fe_3O_4 NP (blue), Fe_3O_4/SiO_2 core/shell nanoparticles (black) and Au@Fe_3O_4/SiO_2 core shell nanoparticles (red). **(c)** UV-Vis spectrum showing the normalized absorption of citrate stabilized Au NP (black) and Au@Fe_3O_4/SiO_2 core shell nanoparticles (red). **(d)** Representative SEM image of the Au@Fe_3O_4/SiO_2 NPs. Small AuNPs are clearly visible on the surface of SiO_2 spheres.**(e)**EDS patterns of Au@Fe_3O_4/SiO_2 NPs confirming the presence of Au, Fe and Si in our nanohybrid system.

The as synthesized Au@Fe$_3$O$_4$/SiO$_2$ NPs were further characterized by Dynamic Light scattering **(Figure3.9)**. We can clearly see a steady increase in the hydrodynamic diameter of NPs upon coating of SiO$_2$ shell and adsorption of AuNPs over the SiO$_2$ shell.
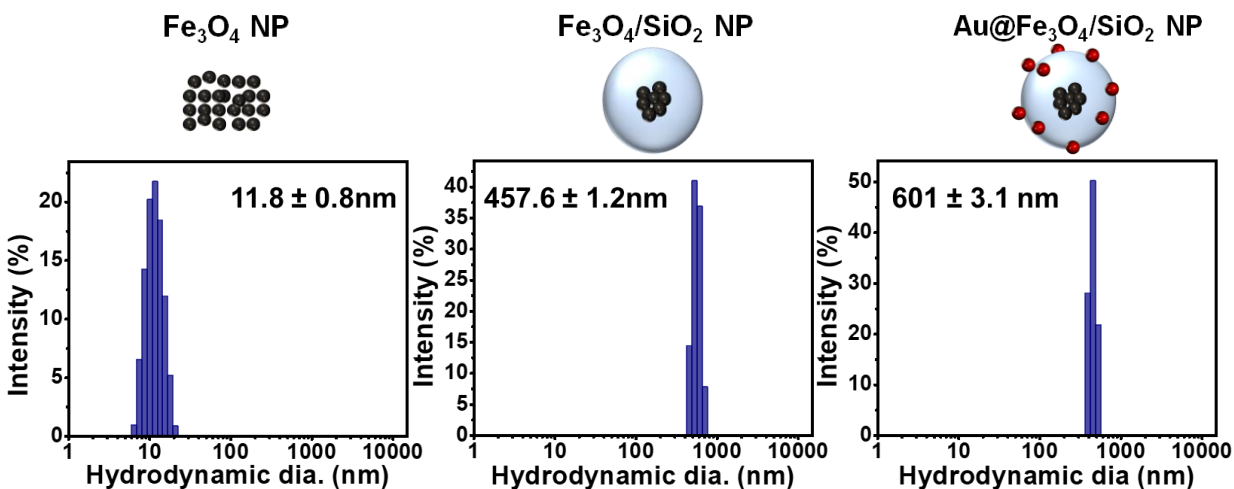
Figure 3.9|DLS spectra of Fe$_3$O$_4$, Fe$_3$O$_4$/SiO$_2$ and Au@Fe$_3$O$_4$/SiO$_2$ NPs. DLS measurements show a steady increase in the hydrodynamic diameter of NPs, indicating the growth of SiO$_2$ shell and then adsorption of AuNPs.

3.2.3. Catalytic reduction of 4-Nitrophenol: Since the prepared plasmonic-magnetic system displayed AuNPs on its surface, we planned to use them for AuNP catalyzed reductions (**Figure 3.10**).The most attractive feature of the prepared structure being the easy recovery of the catalyst from the solution (~10 mins) with the use of a magnet. We chose the catalytic reduction of 4-nitrophenol (PNP) in the presence of NaBH$_4$, as our model reaction. This reaction is attractive as **(a)** the progress of the reaction can be monitored by UV-Vis. studies, where PNP (the reactant) has a prominent peak at ~ 400nm, and 4-aminophenol (PNA, the product) displays a peak at ~300nm, **(b)** the presence of AuNPs is crucial as the reaction does not proceed in the absence of AuNPs. Here, AuNPs act as a mediator of hydride (H$^-$) transfer between BH$_4^-$ and PNP in accordance with Langmuir–Hinshelwood mechanism[18]. According to this mechanism, metal nanoparticles act as a substrate for H$^-$, thereby, facilitating the reduction. Typically, the reaction proceeds with PNP getting adsorbed on the NP surface, which is rich in H$^-$ (from NaBH$_4$).The adsorbed H$^-$, then reduces PNP to PNA, which is the rate

determining step of the reaction. The PNA, once formed, gets desorbed from the surface of NPs, rendering the active site available for next cycle of catalysis.
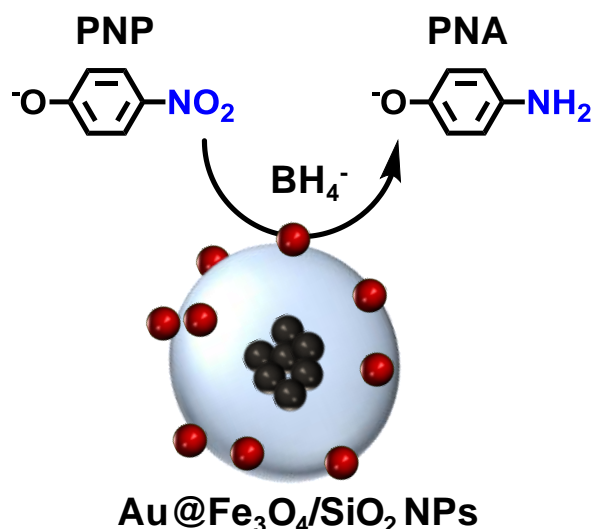
Figure 3.10| Schematic illustration of 4-nitrophenol (PNP) reduction to 4-aminophenol (PNA) with Au@Fe$_3$O$_4$/SiO$_2$ NPs as the catalyst.

We observed a swift reduction in the peak intensity of PNA, with (~4nM in terms of AuNPs) Au@Fe$_3$O$_4$/SiO$_2$ NPs as the catalyst (within ~10mins) (**Figure 3.11 (a), (b)**). The reduction process, where the solution color transformed from yellow to colorless, was monitored using UV-Vis. spectroscopy, where the peak corresponding to PNP (at ~400nm) decreased steadily with a concomitant increase in a peak at ~300nm, corresponding to the formation of PNA. The presence of isosbestic points clearly shows transformation of the reactant to a single product (PNP in our case).We performed time-dependent UV-Vis. experiments in order to get quantitative details regarding the kinetics of the reaction. **Figure 3.11 (c)** shows the decrease in PNP peak intensity as a function of time. As the reaction contains ~10 times excess of BH$_4^-$ over PNP, the reaction can be described using a psuedo first order kinetics, as described below[21],

$$PNP + BH_4^- \rightarrow PNA$$

The rate of the reaction is given as,

$$\frac{\text{dPNP}}{\text{dt}} \, \alpha \, [\text{PNP}][\text{BH}_4^-]$$

Since BH$_4$- is present in excess, changes in the concentration of BH$_4^-$ can be taken as zero. Thus, the resulting rate law is given as,

$$\frac{\text{dPNP}}{\text{dt}} \, \alpha \, [\text{PNP}]$$

Here, the reaction is first order in PNP and zero order in BH$_4^-$.

In order to get the value of the rate constant (k) for this reaction, we integrated the above rate law to get the following integrated rate equation.

$$-\ln\left(\frac{c_t}{c_0}\right) = k.t$$

Here,

c_t is the concentration of PNP at time t

c_o is the initial concentration of PNP

k is the rate constant.

A plot between –ln(c_t/c_0) and t will be a straight line with an intercept zero, and slope, being equal to the rate constant (k). We, therefore plotted the data in an integrated first order equation and got the rate constant (k) of ~0.24min^{-1}(**Figure 3.11 (d)**).
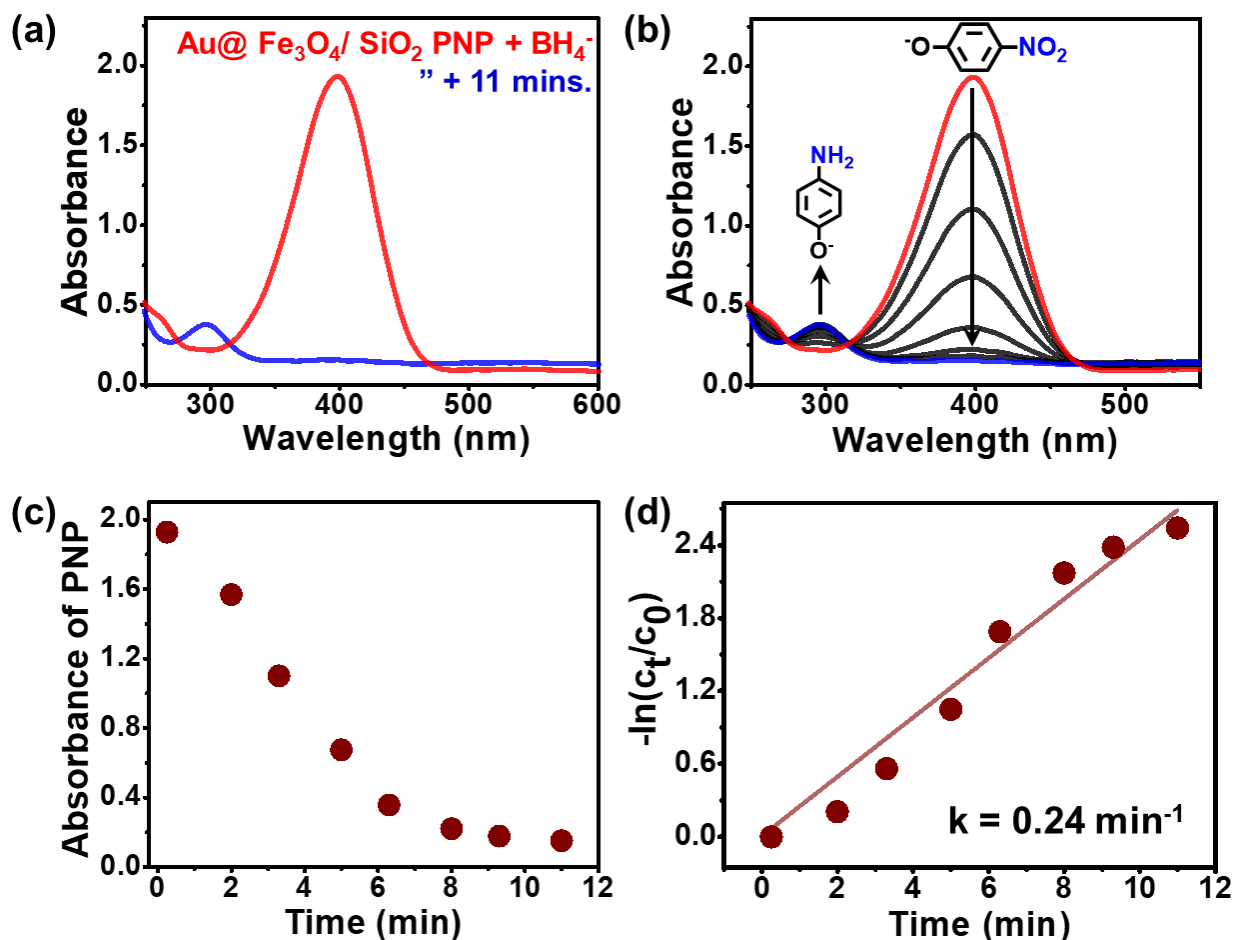
Figure 3.11| Au@Fe$_3$O$_4$/SiO$_2$ catalyzed PNP reduction. **(a)** UV-Vis spectrum of PNP before the addition of nanoparticles (red) and after catalysis (black). The sharp decline of the PNP absorbance peak around ~400 nm was observed after the addition of nanoparticles (~4nM in terms of AuNPs). **(b)**The entire catalytic cycle of PNP reduction. A gradual decrease in the nitrophenolate ion absorbance at 400 nm and a simultaneous emergence of a new peak around 300 nm was observed. **(c)**The progress of PNP reduction. **(d)** Linearized data plot for the first order analysis by monitoring the PNP absorbance around ~400 nm.

Since the AuNPs are adsorbed onto Fe$_3$O$_4$/SiO$_2$ NPs, leading to a decrease in the effective surface area available for catalysis, it is worthwhile to compare the catalytic activity with bare AuNPs of similar concentrations. In lieu of that, we monitored changes in the absorption spectrum of PNP (in 10mM BH$_4^-$), in the presence of citrate stabilized AuNP (~4nm in terms of AuNPs). We observed a similar response where, the intensity of PNP (at ~ 400nm) decreases with time with a concomitant rise in the intensity of PNA (at ~300nm) (**Figure 3.12 (a), (b)**). We also observed the presence of isosbestic points, indicating the transformation of PNP to a single product. Interestingly, both systems

showed comparable catalytic efficiency. We calculated the rate constant for the reaction to be ~0.24min^{-1} with bare AuNPs (**Figure 3.12 (c)**). Note that Fe_3O_4/SiO_2 NPs failed to catalyze PNP reduction (as shown in **Figure 3.12 (d))**confirming the necessity of AuNPs in the catalytic structure.It is important to mention that the rate constants do not show drastic differences on going from homogeneous to heterogeneous catalysis.
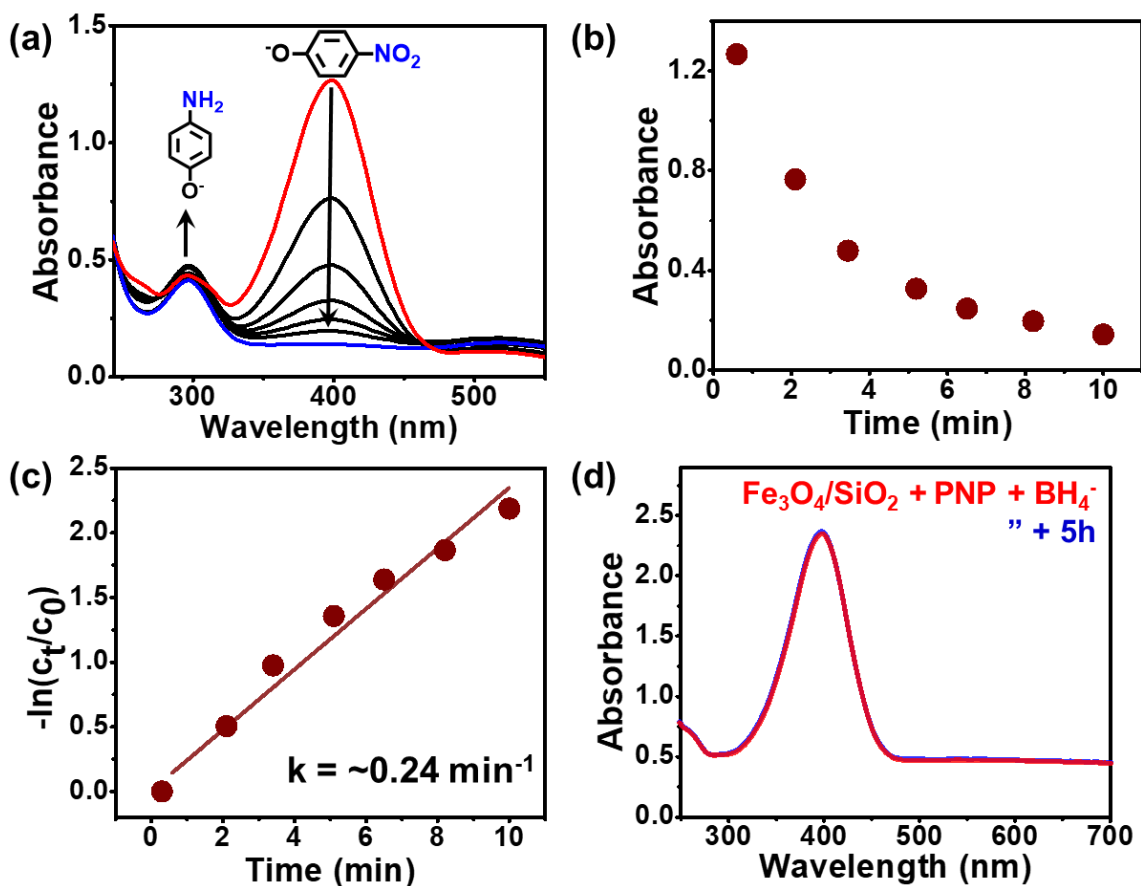
Figure 3.12| Citrate stabilized AuNP catalyzed PNP reduction. (a) UV-Vis. changes accompanying the addition of citrate capped AuNPs (~4nM in terms of AuNPs) to PNP containing 10mM BH_4^-. A complete reduction in the peak intensity at 400nm, corresponding to PNP (reactant) is observed with a concomitant increase in the intensity at 300nm, corresponding to PNA (product). The presence of two isosbestic points indicates the formation of a single product (PNP). **(b)** Variation in the absorption intensity at 400nm (reactant) showing the progress of reduction and**(c)** Corresponding linearized plot.**(d)** PNP reduction using Fe_3O_4/SiO_2 core shell nanoparticles. No reduction was observed here.

The additional flexibility with $Au@Fe_3O_4/SiO_2$ NP over the standard benchmark citrate stabilized AuNP system is the ease of separation of the catalyst after the reduction using a magnet (**Figure 3.13**).
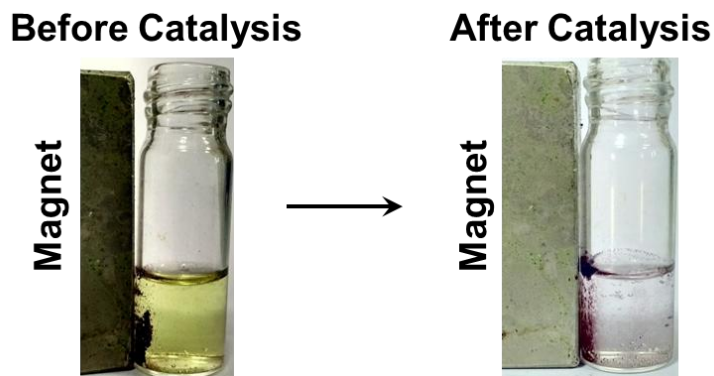
Figure 3.13| Photograph of Au@Fe$_3$O$_4$/SiO$_2$ catalyzed PNP reduction. Before the start of the reduction color of the solution was yellow, corresponding to PNP. The yellow color disappeared after catalysis and gold coated magnetic catalyst was recovered via magnetic separation.

This possibility of easy separation of the catalyst allowed us to re-use the catalyst for many more cycles, a task usually not feasible to do with the standard benchmark citrate stabilized AuNP. We washed the catalyst two times with water, and investigated them for cyclability experiments. **Figure 3.14 (a)** shows the cyclability of PNP reduction with Au@Fe$_3$O$_4$/SiO$_2$ catalysts for ~ 10 cycles.Note that the amount of catalyst used for recyclability experiments is higher (~10nM in terms of AuNPs) than what was used for rate calculation experiments. There is a gradual decrease in the catalytic efficiency of each cycle (as indicated by an increase in the time required for completion of each catalytic cycle, **Figure 3.14 (b)**) and this may be attributed to the fact that there is a possibility of desorption of Au NP from the silica surface.

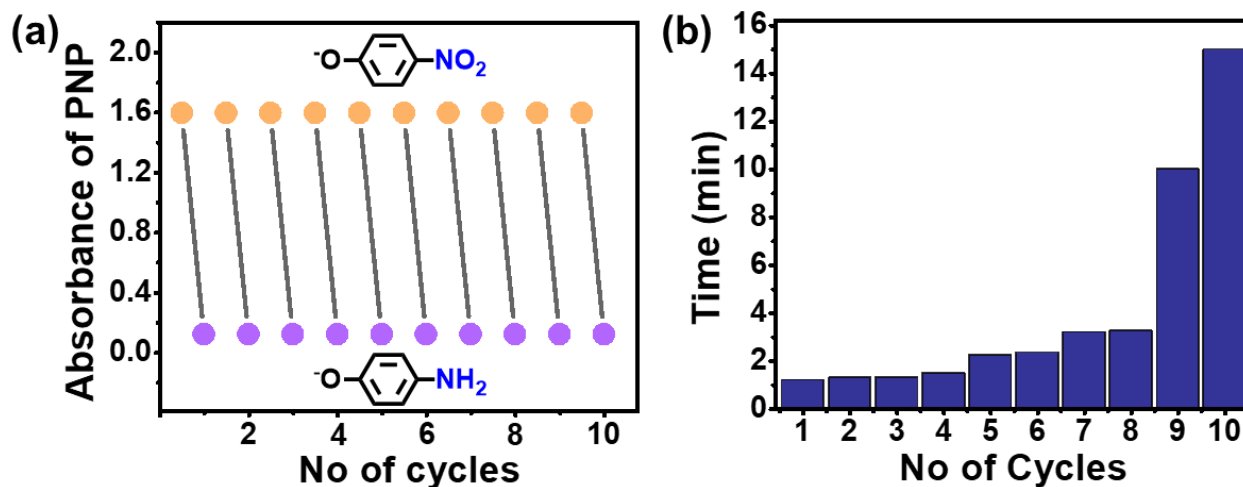**Figure 3.14| Cyclability studies of PNP reduction with Au@Fe₃O₄/SiO₂ NPs. (a)** Variation in the absorption intensity of PNP before the reaction (shown with orange points) and after the reaction (shown in magenta points). **(b)** Variation in the time, required for the complete PNP reduction, as a function of cycles.

A summary of comparisions drawn between PNP reductions with Au@Fe₃O₄/SiO₂ and Au citrate NPs as catalysts is given in the following table.

Nanoparticle System	Rate Constant (min^{-1})	$t_{completion}$ (min)	Cycles
Au@ Fe₃O₄/SiO₂ NPs	0.24	~ 11	10
Au-citrate NPs	~0.24	~ 10	na

Table 3.1|Summary of PNP reduction with Au@Fe₃O₄/SiO₂ and citrate stabilized Au NP catalysts.

From the above table, we can conclude that the prepared hierarchical structure containing both Au and Fe₃O₄ NPs retains the catalytic activity of Au NPs towards PNP reduction. Moreover, the presence of Fe₃O₄ NPs in the core rendered easy magnetic separation of the catalyst from the products. Thus, the catalyst, therefore, could be used for multiple times.

3.2.4. Photo-catalytic reduction of Ferricyanide: Plasmonic photocatalysis is one of emerging applications of metal nanoparticles[19]. To investigate the plasmonic photocatalytic efficiency of our designed material (Au@Fe₃O₄/SiO₂ NPs), we studied the one-electron reduction of ferricyanide ($[Fe(CN)_6]^{3-}$) to ferrocyanide ($[Fe(CN)_6]^{4-}$), which has been catalyzed by transition metal nanostructures, including Au nanoparticles (**Figure 3.15**). The catalytic reduction of $[Fe(CN)_6]^{3-}$ using strong reducing agent such as NaBH₄ and AuNP as catalyst have been extensively studied in the literature[19]. Here, AuNPs act as a reservoir of electrons (a nanoelectrode) from the strong reducing agent NaBH₄.$[Fe(CN)_6]^{3-}$ions will get adsorbed on the surface of nanoparticle and the electrons are supplied by the NP, leading to the reduction of $[Fe(CN)_6]^{3-}$ to $[Fe(CN)_6]^{4-}$. It has been shown that the negative potential of metal particle is facilitating the reduction of $[Fe(CN)_6]^{3-}$ions[19].Recently, it has been shown that the reduction happens upon photo irradiation without the necessary use of a reducing agent like NaBH₄[19].
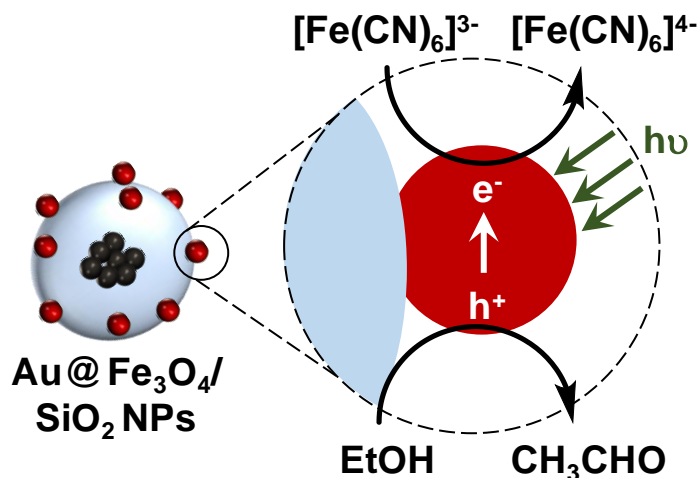
Figure 3.15| Schematic illustration of photocatalytic single electron reduction of $[Fe(CN)_6]^{3-}$ to $[Fe(CN)_6]^{4-}$ with Au@Fe$_3$O$_4$/SiO$_2$ NPs as the catalyst.

Visible light photo-excitation of AuNPs generates high energy electrons in the conduction band of AuNPs (also known as hot electrons), which reduce the $[Fe(CN)_6]^{3-}$ ions that get adsorbed on the nanoparticle surface.

$$[Fe(CN)_6]^{3-} + e^-_{Au} \rightarrow [Fe(CN)_6]^{4-}$$
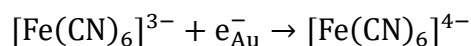
The holes generated in the valence band, as a result of photo excitation areneutralized using a hole scavenger (like ethanol, EtOH). The activation barrier for the reaction is less in presence of light compared to dark conditions. This indicates that the photo excitation of gold nanoparticles enhances the electron transfer for the reduction[19].

We followed the photo-catalytic reduction of $[Fe(CN)_6]^{3-}$ ions spectrophotometrically by looking at the absorption changes as a function of irradiation time. Argon was purged into the solution mixture in order to ensure the anaerobic conditions. Absorbance of $[Fe(CN)_6]^{3-}$ was monitored every 15 minutes.We observed a gradual decrease in the absorption of $[Fe(CN)_6]^{3-}$ at ~420 nm and a concomitant increase in absorbance at 240nm indicating the reduction of $[Fe(CN)_6]^{3-}$ to $[Fe(CN)_6]^{4-}$ (**Figure 3.16 (a)**). The decrease in the absorption intensity at ~420nm, as a function of time, is plotted in **Figure 3.16 (b)**. Further, we plotted the data in an integrated first

order equation and estimated the rate constant (k) to be~ 0.007min^{-1} (**Figure 3.16 (c)**).Control experiment, performed under similar conditions, but in the absence of photoexcitation, failed to show any measurable catalysis by our catalyst (**Figure3.16 (d)**). This confirmed the necessity of photo-excited electrons from AuNPs to catalyze the reduction reaction.
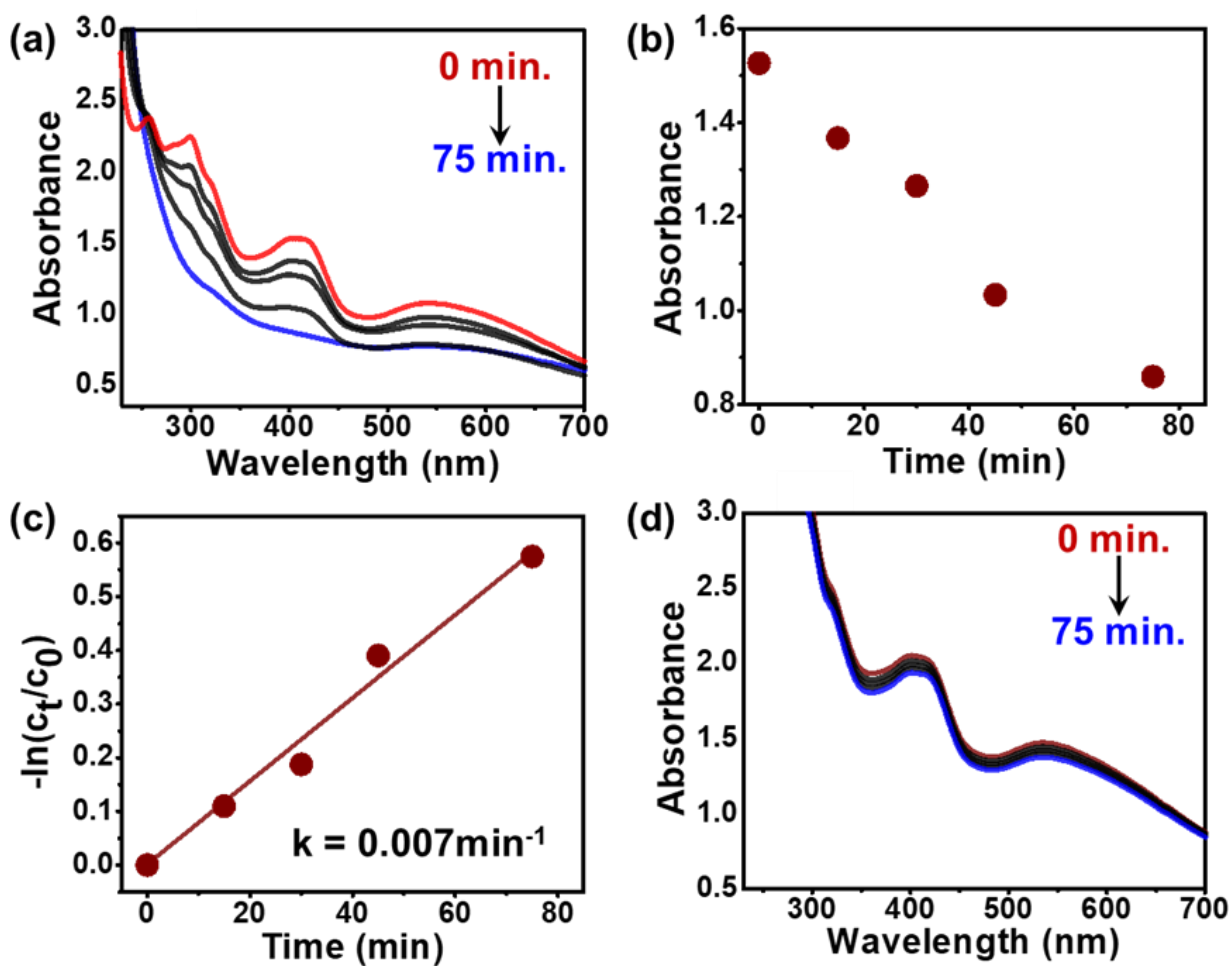
Figure3.16| Photocatalytic reduction of [Fe(CN)$_6$]$^{3-}$by Au@Fe$_3$O$_4$/SiO$_2$ NPs.(a) Photocatalytic reduction of [Fe(CN)$_6$]$^{3-}$by monitoring the absorption changes at 15min interval in the presence of Au@Fe$_3$O$_4$/SiO$_2$ NPs. **(b)** Progress of reduction.**(c)** Linearized data plot for the first order analysis by tracking the change in absorbance of [Fe(CN)$_6$]$^{3-}$ at 420nm. **(d)** Control experiment in which reaction is carried out under dark conditions, i.e. without photoexcitation. No noticeable reduction was observed.

To compare the photo-catalytic efficiency of AuNPs chemisorbed onto Fe$_3$O$_4$/SiO$_2$ NPs versus AuNPs in solution, we performed another set of reduction reactions, with citrate capped AuNPs as catalysts. **Figure 3.17 (a)** shows changes in theUV-Vis. absorption

spectrum as a function of irradiation time. Upon plotting the data in integrated first order equation (**Figure 3.17 (b)**), we found the rate constant for catalysis by citrate capped AuNPs ($0.008min^{-1}$) to be similar to that of Au@Fe_3O_4/SiO_2 NPs ($0.007min^{-1}$). The comparisons drawn between the homogeneous and heterogeneous catalysis are summarized in **Figure 3.17 (c)**.

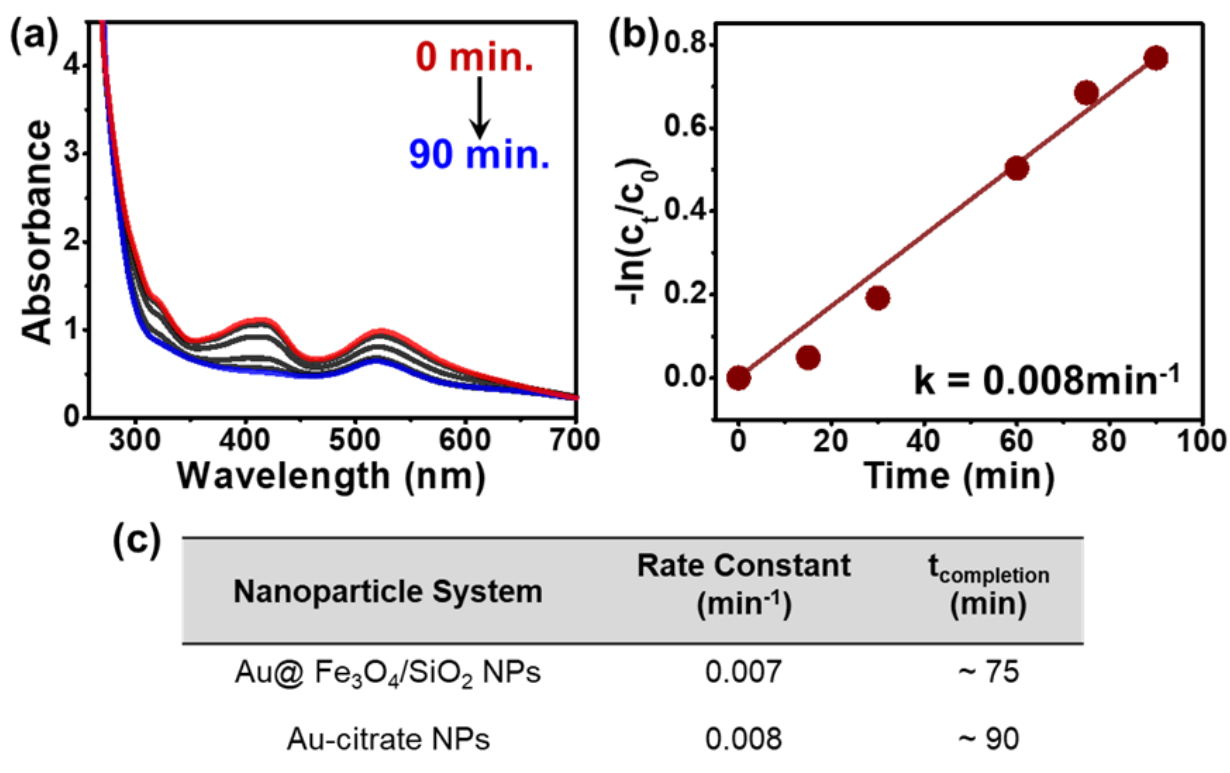| Nanoparticle System	Rate Constant (min^{-1})	$t_{completion}$ (min)
Au@ Fe_3O_4/SiO_2 NPs	0.007	~ 75
Au-citrate NPs	0.008	~ 90

Figure 3.17| Photocatalytic reduction of [Fe(CN)$_6$]$^{3-}$by citrate stabilized AuNP. (a) Photocatalytic reduction of $[Fe(CN)_6]^{3-}$ by monitoring the absorption changes at 15min interval in the presence of citrate stabilized AuNP. **(b)** Linearized data plot for the first order analysis by tracking the change in absorbance of $[Fe(CN)_6]^{3-}$ at 420nm. **(c)** Comparison of $[Fe(CN)_6]^{3-}$photoreduction by citrate stabilizedAuNP and Au@ Fe_3O_4/SiO_2 NP catalysts.

In order to characterize the product of the photocatalytic reduction reaction ($[Fe(CN)_6]^{4-}$), we did Prussian blue identification test[22] (**Figure 3.18)**. It is well known that potassium ferrocyanide ($[Fe(CN)_6]^{4-}$), upon reacting with Fe(III), yields a Prussian blue pigment with the chemical identity $KFe^{III}[Fe^{II}(CN)_6]$.A similar reaction between $[Fe(CN)_6]^{4-}$ and Fe(III) fails to give Prussian blue color before the reaction.

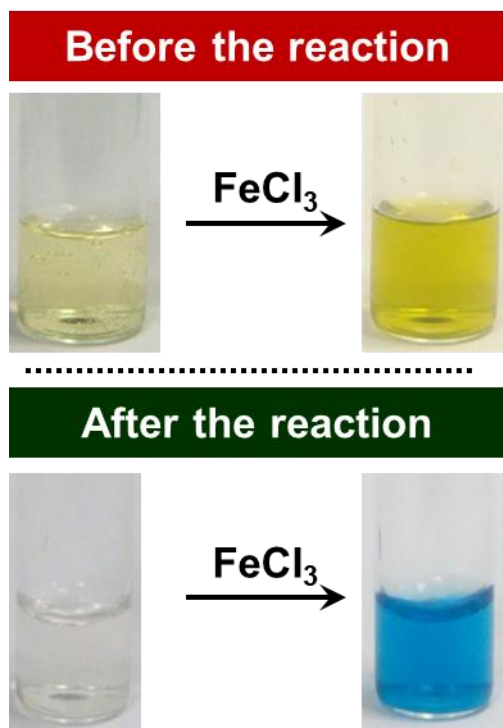**Figure 3.18| Characterization of the product ([Fe(CN)$_6$]$^{4-}$).**Prussian blue test indicating the formation of Fe(II) after the photocatalytic reduction of [Fe(CN)$_6$]$^{3-}$. Here, only the reaction between potassium ferrocyanide (the product) and Fe(III) results in the formation of Prussian blue complex.

Chapter 4: Conclusion

In the present thesis, we summarized our recent endeavor towards the introduction of advanced functional traits to particles at the nanoscale. Here, we attempted to integrate two highly desirable properties, namely the existence of plasmons and possession of magnetic activity into a core/shell NP geometry. Our inability to synthesize the proposed structure, possibly due to the high lattice mismatch between Fe_3O_4 and Au nanoparticles, prompted us to undertake a slightly different strategy. With that goal in mind, we devoted our efforts to synthesize a multi-component hierarchical material with Fe_3O_4 as the core material and a SiO_2 shell covering the core. AuNPs were then incorporated over the mesoporous SiO_2 shell by the help of amine functionalization. Aftersuccessfully demonstrating the synthesis of the desired material, we studied its use for NP catalyzed reductions. We show that despite having lower surface area than homogeneous solution of AuNPs, our hierarchical structure displayed comparable catalytic rates. Moreover, the recovery of the catalyst was an easy task because of magnetic separation. The present method of integrating multifunctions into a single nanostructure is general and allows one to use any combination of materials. These kind of multifunctional materials serves as an exciting and promising platform for nanoparticle based applications in therapeutics and diagnosis.

References

(1)   Chen, N.; He, Y.; Su, Y.; Li, X.; Huang, Q.; Wang, H.; Zhang, X.; Tai, R.; Fan, C. The Cytotoxicity of Cadmium-Based Quantum Dots. *Biomaterials* **2012**, *33* (5), 1238–1244.

(2)   Jana, J.; Ganguly, M.; Pal, T. Enlightening Surface Plasmon Resonance Effect of Metal Nanoparticles for Practical Spectroscopic Application. *RSC Adv.* **2016**, *6* (89), 86174–86211.

(3)   Amendola, V.; Pilot, R.; Frasconi, M.; Maragò, O. M.; Iatì, A. M. Surface Plasmon Resonance in Gold Nanoparticles: A Review. *J. Phys. Condens. Matter* **2017**, *29* (20), 203002.

(4)   Luther, J. M.; Jain, P. K.; Ewers, T.; Alivisatos, A. P. Localized Surface Plasmon Resonances Arising from Free Carriers in Doped Quantum Dots. *Nat. Mater.* **2011**, *10* (5), 361–366.

(5)   http://www.educatedtherapists.com

(6)   Li, J.; Zhao, T.; Chen, T.; Liu, Y.; Ong, C. N.; Xie, J. Engineering Noble Metal Nanomaterials for Environmental Applications. *Nanoscale* **2015**, *7* (17), 7502–7519.

(7)   Bronstein, L. M.; Huang, X.; Retrum, J.; Schmucker, A.; Pink, M.; Stein, B. D.; Dragnea, B. Influence of Iron Oleate Complex Structure on Iron Oxide Nanoparticle Formation. *Chem. Mater.* **2007**, *19* (15), 3624–3632.

(8)   Xu, Z.; Hou, Y.; Sun, S. Magnetic Core/Shell Fe 3 O 4 /Au and Fe 3 O 4 /Au/Ag Nanoparticles with Tunable Plasmonic Properties. *J. Am. Chem. Soc.* **2007**, *129* (28(1) Xu, Z.; Hou, Y.; Sun, S. Magnetic Core/Shell Fe 3 O 4 /Au and Fe 3 O 4 /Au/Ag Nanoparticles with Tunable Plasmonic Properties. J. Am. Chem. Soc. 2007, 129 (28), 8698–8699.), 8698–8699.

(9)   Malyutin, A. G.; Easterday, R.; Lozovyy, Y.; Spilotros, A.; Cheng, H.; Sanchez-

Felix, O. R.; Stein, B. D.; Morgan, D. G.; Svergun, D. I.; Dragnea, B.; et al. Viruslike Nanoparticles with Maghemite Cores Allow for Enhanced Mri Contrast Agents. *Chem. Mater.* **2015**, *27* (1), 327–335.

(10)   Yan, Y.; Timonen, J. V. I.; Grzybowski, B. A. A Long-Lasting Concentration Cell Based on a Magnetic Electrolyte. *Nat. Nanotechnol.* **2014**, *9* (11), 901–906.

(11)   Yang, J.; Sargent, E. H.; Kelley, S. O.; Ying, J. Y. A General Phase-Transfer Protocol for Metal Ions and Its Application in Nanocrystal Synthesis. *Nat. Mater.* **2009**, *8* (8), 683–689.

(12)   Banerjee, S.; Raja, S. O.; Sardar, M.; Gayathri, N.; Ghosh, B.; Dasgupta, A. Iron Oxide Nanoparticles Coated with Gold: Enhanced Magnetic Moment due to Interfacial Effects. *J. Appl. Phys.* **2011**, *109* (12).

(13)   Woo, E.; Ponvel, K. M.; Ahn, I.; Lee, C. Synthesis of Magnetic / Silica Nanoparticles with a Core of Magnetic Clusters and Their Application for the Immobilization of His-Tagged Enzymes. *J. Mater. Chem.* **2010**, 1511–1515.

(14)   Insin, N.; Tracy, J. B. J.; Lee, H.; Zimmer, J. P. J.; Westervelt, R. M.; Bawendi, M. G. Incorporation of Iron Oxide Nanoparticles and Quantum Dots into Silica Microspheres. *ACS Nano* **2008**, *2* (2), 197–202.

(15)   Ertem, E.; Murillo-Cremaes, N.; Carney, R. P.; Laromaine, A.; Janeček, E.-R.; Roig, A.; Stellacci, F. A Silica-Based Magnetic Platform Decorated with Mixed Ligand Gold Nanoparticles: A Recyclable Catalyst for Esterification Reactions. *Chem. Commun.* **2016**, *52* (32), 5573–5576.

(16)   Turkevich, J.; Stevenson, P. C. A Study of the Nucleation and Growth Processes In the Synthesis of Colloidal Gold. *Discuss.Faraday Soc.* **1951**, 11, 55.

(17)   Pastoriza-santos, I.; Gomez, D.; Pe, J. Optical properties of metal nanoparticles coated silica spheres: a simple effective medium approach. PCCP. **2004**, 6, 5056–5060.

(18)   Roy, S.; Rao, A.; Devatha, G.; Pillai, P. P. Revealing the Role of Electrostatics in

Gold-Nanoparticle-Catalyzed Reduction of Charged Substrates. *ACS Catal.* **2017**, *7* (10), 7141–7145.

(19) Kim, Y.; Dumett Torres, D.; Jain, P. K. Activation Energies of Plasmonic Catalysts. *Nano Lett.* **2016**, *16* (5), 3399–3407.

(20) Kostevsek, N.; Locatelli, E.; Garrovo, C.; Arena, F.; Monaco, I.; Nikolov, I. P.; Sturm, S.; Zuzek Rozman, K.; Lorusso, V.; Giustetto, P.; et al. The One-Step Synthesis and Surface Functionalization of Dumbbell-like Gold–iron Oxide Nanoparticles: A Chitosan-Based Nanotheranostic System. *Chem. Commun.* **2016**, *52* (2), 378–381.

(21) Hervés, P.; Pérez-Lorenzo, M.; Liz-Marzán, L. M.; Dzubiella, J.; Lu, Y.; Ballauff, M. Catalysis by Metallic Nanoparticles in Aqueous Solution: Model Reactions. *Chem. Soc. Rev.* **2012**, *41* (17), 5577.

(22) Pharmacopoeia, E. Chapter Three. In *Telemedicine Journal*; 1995; Vol. 1, pp 347–350.